A&A 613, A55 (2018)
https://doi.org/10.1051/0004-6361/201731974

Astronomy & Astrophysics

Structure of the Balmer jump

The isolated hydrogen atom

F. Calvo[1,2], L. Belluzzi[1,3], and O. Steiner[1,3]

[1] Istituto Ricerche Solari Locarno (IRSOL), via Patocchi 57 – Prato Pernice, 6605 Locarno-Monti, Switzerland
e-mail: flavio.calvo@irsol.ch
[2] Geneva Observatory, University of Geneva, Ch. des Maillettes 51, 1290 Sauverny, Switzerland
[3] Kiepenheuer-Institut für Sonnenphysik, Schöneckstrasse 6, 79104 Freiburg, Germany

Received 19 September 2017 / Accepted 3 December 2017

ABSTRACT

Context. The spectrum of the hydrogen atom was explained by Bohr more than one century ago. We revisit here some of the aspects of the underlying quantum structure, with a modern formalism, focusing on the limit of the Balmer series.
Aims. We investigate the behaviour of the absorption coefficient of the isolated hydrogen atom in the neighbourhood of the Balmer limit.
Methods. We analytically computed the total cross-section arising from bound-bound and bound-free transitions in the isolated hydrogen atom at the Balmer limit, and established a simplified semi-analytical model for the surroundings of that limit. We worked within the framework of the formalism of Landi Degl'Innocenti & Landolfi (2004, Astrophys. Space Sci. Lib., 307), which permits an almost straight-forward generalization of our results to other atoms and molecules, and which is perfectly suitable for including polarization phenomena in the problem.
Results. We analytically show that there is no discontinuity at the Balmer limit, even though the concept of a "Balmer jump" is still meaningful. Furthermore, we give a possible definition of the location of the Balmer jump, and we check that this location is dependent on the broadening mechanisms. At the Balmer limit, we compute the cross-section in a fully analytical way.
Conclusions. The Balmer jump is produced by a rapid drop of the total Balmer cross-section, yet this variation is smooth and continuous when both bound-bound and bound-free processes are taken into account, and its shape and location is dependent on the broadening mechanisms.

Key words. atomic processes – opacity

1. Introduction

This paper contains the first step of a work whose final goal is the numerical modelling of the Balmer jump in both the intensity and the linearly polarized spectrum of the solar radiation. Here, we investigate the behaviour of the absorption coefficient around the limit of the Balmer series, under the assumption of an isolated hydrogen atom (i.e., an atom that does not interact with any other particle) and in the absence of magnetic fields.

A numerical calculation of the absorption coefficient of the hydrogen atom near the Balmer limit, including both bound-bound and bound-free processes, was carried out by Stenflo (2005). There, the oscillator strengths (which are directly related to the Einstein B coefficients) are computed from the Gaunt factors, which have historically been tabulated, and for which approximate formulas have been derived for quick computations. Thanks to the increased computational power available today, we have opted for a different approach in this work: we start from the analytical expression of the wavefunctions of electrons and compute oscillator strengths by evaluating the radial integrals numerically. With this approach, we are no longer bound to existing tables or approximate formulas.

It must be observed that the radial integrals for the hydrogen atom have also been computed analytically, and the result expressed in a closed form (Gordon 1929). A generalized expression for hydrogenic atoms was later proposed by Menzel & Pekeris (1935), although without any proof. Almost thirty years later, Menzel (1964) provided the proof, in a simpler and more elegant way than in Gordon (1929). A closed formula for the evaluation of the oscillator strengths has therefore long been available. It requires the evaluation of hypergeometric functions, however, which can be troublesome near the series limits. As we show below, difficulties near the series limits are also met with the numerical integration methods that are developed in this work, but these methods have the advantage of being directly applicable to more complex electron wavefunctions.

The most exhaustive study of the hydrogen atom we found was performed in Bethe & Salpeter (1957), but we prefer to refer, whenever possible, to Landi Degl'Innocenti & Landolfi (2004) and more recent textbooks in order to keep a standard and more recent notation and formalism.

The structure of this contribution is as follows. In Sect. 2 we provide the explicit expression of the bound-bound and bound-free absorption coefficients in terms of the density of quantum states and the Einstein B coefficients. Sect. 3 is devoted to the computation of the density of quantum states, whereas Sect. 4 is dedicated to the formal computation of the Einstein coefficients from the analytic expression of the wavefunctions of the free and bound electrons. In Sect. 5 we match the absorption

bound-bound and bound-free coefficients below and above the Balmer limit, respectively, and we analytically show that there is no discontinuity. In addition, we analytically compute the cross-section at that precise point. Sect. 6 is a preliminary numerical calculation of the total cross-section (bound-bound and bound-free processes from the $n = 2$ level) around the Balmer limit, taking only natural and thermal broadening into account.

2. Absorption coefficient

We consider a multi-level atom, and we work within the framework of the formalism of Landi Degl'Innocenti & Landolfi (2004). Each energy level is specified by the quantum numbers (αJ), with J the total angular momentum, and α a set of inner quantum numbers. In the absence of magnetic fields and neglecting stimulated emission, the absorption coefficient due to bound-bound transitions is given by Eq. (7.16a) of Landi Degl'Innocenti & Landolfi (2004):

$$[\eta_i(\nu,\boldsymbol{\Omega})]_{\rm bb} = \frac{h\nu}{4\pi}\mathcal{N}\sum_{\alpha_\ell J_\ell}\sum_{\alpha_u J_u}(2J_\ell+1)\,B(\alpha_\ell J_\ell\rightarrow\alpha_u J_u) \times\sum_{KQ}\sqrt{3}\,(-1)^{1+J_\ell+J_u+K}\left\{\begin{array}{ccc}1 & 1 & K\\ J_\ell & J_\ell & J_u\end{array}\right\} \times\mathcal{T}^K_Q(i,\boldsymbol{\Omega})\,\rho^K_Q(\alpha_\ell J_\ell)\,\phi_{\rm bb}(\nu_{u\ell}-\nu), \quad (1)$$

where ν is the frequency of the radiation, $\boldsymbol{\Omega}$ is the propagation direction, and where the index i can take values 0, 1, 2, and 3, standing for Stokes I, Q, U, and V, respectively. The quantity h is the Planck constant, $\mathcal{N}$ is the number density of atoms, $B(\alpha_\ell J_\ell \rightarrow \alpha_u J_u)$ is the Einstein coefficient for absorption from a lower level $(\alpha_\ell J_\ell)$ to an upper level $(\alpha_u J_u)$, $\mathcal{T}^K_Q(i,\boldsymbol{\Omega})$ is the polarization tensor (see Table 5.6 in Landi Degl'Innocenti & Landolfi 2004), and $\rho^K_Q(\alpha_\ell J_\ell)$ are the multipolar components of the density matrix (or spherical statistical tensors) of the lower level. In the atomic reference frame, the absorption profile $\phi_{\rm bb}(\nu_{u\ell}-\nu)$ is a Lorentzian, with $\nu_{u\ell}$ the transition frequency defined by

$$\nu_{u\ell} = \frac{E_u - E_\ell}{h}, \quad (2)$$

with E_u and E_ℓ the energies of levels $(\alpha_u J_u)$ and $(\alpha_\ell J_\ell)$, respectively. The threshold frequency for photoionization from a given lower level is

$$\nu_{\rm th}(\alpha_\ell J_\ell) = \frac{E_{\alpha_+ J_+} - E_\ell}{h}, \quad (3)$$

with $E_{\alpha_+ J_+}$ the energy of the level $(\alpha_+ J_+)$ in which the ion is left after photoionization. Indicating with ϵ_u the (negative) energy of the upper level $(\alpha_u J_u)$ in a energy scale in which $E_{\alpha_+ J_+} = 0$, the transition frequency $\nu_{u\ell}$ can be written as

$$\nu_{u\ell} = \nu_{\rm th}(\alpha_\ell J_\ell) + \frac{\epsilon_u}{h}. \quad (4)$$

If the lower level is not polarized, then (see Eqs. (10.6) and (10.7) in Landi Degl'Innocenti & Landolfi 2004 for more details)

$$\rho^K_Q(\alpha_\ell J_\ell) = \delta_{K0}\,\delta_{Q0}\,\frac{1}{\sqrt{2J_\ell+1}}\,\frac{\mathcal{N}_{\alpha_\ell J_\ell}}{\mathcal{N}}, \quad (5)$$

with $\mathcal{N}_{\alpha_\ell J_\ell}$ the number density of atoms in the lower level. Substituting Eq. (5) into Eq. (1), observing that $\mathcal{T}^0_0(i,\boldsymbol{\Omega}) = \delta_{i0}$, and using the analytical expression of the 6-j symbols when one of the arguments is zero (see Eq. (2.36a) in Landi Degl'Innocenti & Landolfi 2004), we obtain the familiar expression

$$[\eta_i(\nu)]_{\rm bb} = \delta_{i0}\,\frac{h\nu}{4\pi}\sum_{\alpha_\ell J_\ell}\mathcal{N}_{\alpha_\ell J_\ell} \times\sum_{\alpha_u J_u}B(\alpha_\ell J_\ell\rightarrow\alpha_u J_u)\,\phi_{\rm bb}\left(\nu_{\rm th}(\alpha_\ell J_\ell)+\frac{\epsilon_u}{h}-\nu\right). \quad (6)$$

As expected, in the absence of magnetic fields, and assuming that the lower level is unpolarized, only the absorption coefficient for the intensity ($i = 0$) is non-zero, and it does not depend on the propagation direction of the radiation.

The absorption coefficient for bound-free transitions (in the absence of atomic polarization in the lower level) can be easily obtained in a similar way as Eq. (6):

$$[\eta_i(\nu)]_{\rm bf} = \delta_{i0}\,\frac{h\nu}{4\pi}\sum_{\alpha_\ell J_\ell}\mathcal{N}_{\alpha_\ell J_\ell} \times\int_0^\infty {\rm d}\epsilon\,\mathcal{N}_{\rm f}(\epsilon)\sum_{ljJ'}B(\alpha_\ell J_\ell\rightarrow\alpha_+ J_+,\epsilon l j,J') \times\phi_{\rm bf}\left(\nu_{\rm th}(\alpha_\ell J_\ell)+\frac{\epsilon}{h}-\nu\right), \quad (7)$$

where $(\alpha_\ell J_\ell)$ is the bound level of the atom from which photoionization takes place, $(\alpha_+ J_+)$ is the level at which the ion is left, ϵ is the (positive) energy of the released electron, l and j are its orbital and total angular momentum, respectively, and J' is the total angular momentum of the final state ($\boldsymbol{J'} = \boldsymbol{J_+} + \boldsymbol{j}$). The quantity $\mathcal{N}_{\rm f}(\epsilon)$ is the number density of quantum states of the free electron with energy ϵ. The profile $\phi_{\rm bf}$ can be defined similarly as the line profile $\phi_{\rm bb}$, but its exact shape is irrelevant in the following derivations.

We now particularize our formalism to the case of the hydrogen atom, which we describe neglecting the spin and relativistic corrections. In this case, the atomic states are specified by the quantum numbers (nl), with n the principal quantum number ($n \geq 1$), and l the orbital angular momentum (or azimuthal quantum number, $0 \leq l \leq n-1$). The energies of the levels depend on the principal quantum number n alone. The degeneracy of the levels is $g(n) = n^2$. Indicating with (nl) the initial bound state, with $(n_u l_u)$ a given upper bound state, and with (ϵl_f) an arbitrary free state with positive energy ϵ, we have

$$[\eta(\nu)]_{\rm bb} = \frac{h\nu}{4\pi}\sum_{nl}\mathcal{N}_{nl} \times\sum_{n_u l_u}B(nl\rightarrow n_u l_u)\,\phi_{\rm bb}\left(\nu_{\rm th}(n)+\frac{\epsilon_u}{h}-\nu\right), \quad (8)$$

and

$$[\eta(\nu)]_{\rm bf} = \frac{h\nu}{4\pi}\sum_{nl}\mathcal{N}_{nl} \times\sum_{l_f}\int {\rm d}\epsilon\,\mathcal{N}_{\rm f}(\epsilon)\,B(nl\rightarrow\epsilon l_f)\,\phi_{\rm bf}\left(\nu_{\rm th}(n)+\frac{\epsilon}{h}-\nu\right), \quad (9)$$

where we have dropped the index i, since only the absorption coefficient for the intensity is non-zero.

Near the photoionization limit, the bound states asymptotically approach the limit forming a quasi-continuum, so that the sum over the upper levels (n_u) in Eq. (8) can be formally substituted with an integral

$$\sum_{n_u} B(nl \to n_u l_u)\, \phi_{\rm bb}\left(\nu_{\rm th} + \frac{\epsilon_u}{h} - \nu\right) \to \int \mathrm{d}\epsilon\, \mathcal{N}_{\rm b}(\epsilon)\, \bar{B}(nl \to \epsilon l_u)\, \phi_{\rm bb}\left(\nu_{\rm th} + \frac{\epsilon}{h} - \nu\right), \quad (10)$$

where $\mathcal{N}_b(\epsilon)$ is the number density of bound states with energy ϵ, and $\bar{B}(nl \to \epsilon l_u)$ is the Einstein coefficient, defined over continuous values of the energy, for the bound-bound transition between the initial level (nl) and the final level with orbital angular momentum l_u and energy ϵ. This Einstein coefficient could be formally obtained by interpolating the Einstein coefficient for the discrete spectrum of upper bound states, but a meaningful continuation of it will later appear in a natural way.

We now focus on the spectral region close to the photoionization threshold from a given lower level n. Close to the photoionization limit, in the frequency interval where the absorption profiles $\phi_{\rm bb}$ and $\phi_{\rm bf}$ significantly contribute to the integral of Eq. (10), the integrand is practically constant. Anticipating the numerical calculations of Sect. 6, we note here that the variation of $\mathcal{N}_{\rm b}(\epsilon)\, \bar{B}(nl \to \epsilon l_u)$ across the wavelength range 3600–3700 Å is linear and as small as 10.5 %. This variation is negligible as compared to the width of the profile, also in a realistic plasma, where due to electron-collisional broadening and other broadening mechanisms (Doppler broadening), the profile is expected to be significantly broader than that of the isolated hydrogen atom. The quantity $\mathcal{N}_{\rm b}(\epsilon)\, \bar{B}(nl \to \epsilon l_u)$ can then be evaluated at the wavelength corresponding to the maximum of the absorption profile $\phi_{\rm bb}$ and factorized out of the integral. We then obtain the following expressions for $[\eta(\nu)]_{\rm bb}$ and $[\eta(\nu)]_{\rm bf}$:

$$[\eta(\nu)]_{\rm bb} = \frac{h^2\nu}{4\pi} \sum_{l l_u} \mathcal{N}_{nl}\, \mathcal{N}_{\rm b}(\epsilon_0)\, \bar{B}(nl \to \epsilon_0 l_u), \quad (11)$$

with $\epsilon_0 = h(\nu - \nu_{\rm th}) < 0$, and

$$[\eta(\nu)]_{\rm bf} = \frac{h^2\nu}{4\pi} \sum_{l l_f} \mathcal{N}_{nl}\, \mathcal{N}_{\rm f}(\epsilon_0)\, B(nl \to \epsilon_0 l_f), \quad (12)$$

with $\epsilon_0 = h(\nu - \nu_{\rm th}) > 0$.

Comparing Eqs. (11) and (12), we see that close to the photoionization limit, the absorption coefficients for bound-bound and bound-free transitions have the same formal expression. The next step is to derive and compare the explicit forms of the density of bound and free states ($\mathcal{N}_{\rm b}(\epsilon)$ and $\mathcal{N}_{\rm f}(\epsilon)$), and of the Einstein coefficients for bound-bound and bound-free transitions.

3. Density of quantum states

On the one hand, the exact form of the density of bound states $\mathcal{N}_{\rm b}$ depends on the way the discrete spectrum of upper states is treated in a continuous manner. On the other hand, as we show below, the density of free states $\mathcal{N}_{\rm f}$ is related to the normalization of the wavefunction of the free electron. To calculate these quantities, as well as the Einstein coefficients, we work in Rydberg units. Then, the energy of the nth bound level of the hydrogen atom is given by

$$\varepsilon_n = -\frac{1}{n^2}, \quad (13)$$

leading to

$$\mathrm{d}\varepsilon = \frac{2}{n^3}\, \mathrm{d}n, \quad (14)$$

and therefore

$$\mathcal{N}_{\rm b}(\varepsilon) \equiv \frac{\mathrm{d}n}{\mathrm{d}\varepsilon} = \frac{n^3}{2}. \quad (15)$$

The determination of the density of quantum states in the free "levels" is more involved, in the sense that the present formalism was developed for transitions to discrete levels, and we are treating a continuous spectrum as a collection of discrete levels in order to stick to the same mathematical tools. Schematically, if we had split the energy range into smaller intervals and picked an approximative wavefunction of the free electron in each interval in order to compute the corresponding Einstein coefficient, the density of quantum states would depend on our splitting. In the limit where those intervals are infinitely small, the density of quantum states will depend on the way the wavefunction of the free electron is normalized. We later choose a normalization for which the density of quantum states is simply

$$\mathcal{N}_{\rm f}(\epsilon) = 1. \quad (16)$$

4. Einstein coefficients

The computation of the Einstein B coefficients is split into two steps. First we express these coefficients as an integral over the wavefunctions of the bound and free electrons. Then we rewrite the wavefunctions of the bound and free electrons in a way that facilitates an analytical integration.

4.1. Reduced matrix elements

The Einstein coefficient for absorption from a lower state specified by the set of quantum numbers (β_ℓ) to an upper state specified by the set (β_u) is given by (e.g. combine Eqs. (7.6) and (7.7) in Landi Degl'Innocenti & Landolfi 2004)

$$B(\beta_\ell \to \beta_u) = \frac{32\pi^4}{3h^2 c}\, |\langle \beta_\ell \,\|\, \boldsymbol{d} \,\|\, \beta_u \rangle|^2, \quad (17)$$

where $\boldsymbol{d} = -e_0 \boldsymbol{r}$ is the dipole operator, and $\langle \cdot \,\|\, \boldsymbol{d} \,\|\, \cdot \rangle$ is the corresponding reduced matrix element. In our case, the bottom line of the problem restricts to the evaluation of the reduced matrix elements $\langle nl \,\|\, \boldsymbol{d} \,\|\, n_u l_u \rangle$ (for bound-bound transitions), and $\left\langle nl \,\|\, \boldsymbol{d} \,\|\, \epsilon l_f \right\rangle$ (for bound-free transitions). As shown in detail in Appendix A, the reduced matrix element for bound-bound transitions is given by

$$\langle nl \,\|\, \boldsymbol{d} \,\|\, n_u l_u \rangle = e_0 (-1)^{l_u+1} \sqrt{(2l_u+1)} \times \begin{pmatrix} l & l_u & 1 \\ 0 & 0 & 0 \end{pmatrix} \mathcal{I}(nl, n_u l_u), \quad (18)$$

where $\mathcal{I}$ is the radial integral defined by

$$\mathcal{I}(nl, n_u l_u) = \int_0^\infty P_{nl}(r)\, r\, P_{n_u l_u}(r)\, \mathrm{d}r, \quad (19)$$

with P_{nl} the reduced radial wavefunction of the bound electron. Similarly, for the bound-free transitions, we have

$$\left\langle nl \,\|\, \boldsymbol{d} \,\|\, \epsilon l_f \right\rangle = e_0 (-1)^{l_f+1} \sqrt{(2l_f+1)} \times \begin{pmatrix} l & l_f & 1 \\ 0 & 0 & 0 \end{pmatrix} \mathcal{I}(nl, \epsilon l_f), \quad (20)$$

with

$$\mathcal{I}(nl, \epsilon l_f) = \int_0^\infty P_{nl}(r)\, r\, \chi_{\epsilon l_f}(r)\, \mathrm{d}r, \tag{21}$$

where $\chi_{\epsilon l_f}(r)$ is the reduced radial wavefunction of the free electron.

4.2. Radial wavefunctions

The normalized radial wavefunctions are found by solving the radial Schrödinger equation for the potential $V(\xi) = -\frac{2}{\xi}$,

$$\left(\frac{\mathrm{d}^2}{\mathrm{d}\xi^2} - \frac{l(l+1)}{\xi^2} - V(\xi) + \varepsilon\right) y = 0, \tag{22}$$

which has been nondimensionalized (or rewritten in Rydberg units) using the substitutions $r = a_0\,\xi$ and $\epsilon = e_0^2\varepsilon/(2a_0)$ with $a_0 = h^2/(4\pi^2 m_e e_0^2)$ the Bohr radius. Taking into account the normalization

$$\int_{\xi=0}^\infty |y(\xi)|^2 \mathrm{d}\xi = \int_{r=0}^\infty |\tilde{y}(r)|^2 \mathrm{d}r = 1, \tag{23}$$

we obtain the transformation law of the wavefunction y under change of variables,

$$y(\xi) = \sqrt{a_0}\tilde{y}(r). \tag{24}$$

Hence the radial integrals (19) and (21) are related to the radial integral in Rydberg units

$$\begin{aligned} \mathcal{J}(nl, n_u l_u) &\equiv \int_0^\infty P_{nl}(\xi)\, \xi\, P_{n_u l_u}(\xi)\, \mathrm{d}\xi, \\ \mathcal{J}(nl, \varepsilon l_f) &\equiv \int_0^\infty P_{nl}(\xi)\, \xi\, \chi_{\varepsilon l_f}(\xi)\, \mathrm{d}\xi, \end{aligned} \tag{25}$$

by the transformations

$$\begin{aligned} \mathcal{I}(nl, n_u l_u) &= a_0\, \mathcal{J}(nl, n_u l_u), \\ \mathcal{I}(nl, \epsilon l_f) &= a_0\, \mathcal{J}(nl, \varepsilon l_f). \end{aligned} \tag{26}$$

For $\varepsilon = -1/n^2 < 0$, the solutions of the radial Schrödinger Eq. (22) can be found in Burgess & Seaton (1960) or in Griffiths (1995):

$$\begin{aligned} P_{nl}(\xi) &= \frac{1}{n} \frac{(-1)^{n+l+1}}{\sqrt{\Gamma(n+l+1)\,\Gamma(n-l)}} W_{n,l+\frac{1}{2}}\left(\frac{2\xi}{n}\right) \\ &= \frac{1}{n}\sqrt{\frac{\Gamma(n-l)}{\Gamma(n+l+1)}} \left(\frac{2\xi}{n}\right)^{l+1} \exp\left(-\frac{\xi}{n}\right) L_{n-l-1}^{(2l+1)}\left(\frac{2\xi}{n}\right), \end{aligned} \tag{27}$$

which are either expressed in terms of the Whittaker W function or in terms of the generalized Laguerre polynomial (whose normalization differs in the literature),

$$L_n^{(\alpha)}(z) = \frac{\Gamma(n+\alpha+1)}{\Gamma(\alpha+1)\Gamma(n+1)}\, {}_1F_1(-n, \alpha+1, z), \tag{28}$$

(see e.g. Abramowitz & Stegun 1964). In turn, the confluent hypergeometric function ${}_1F_1$ can be expressed through the Whittaker M function:

$$M_{\kappa,\mu}(z) = \exp\left(-\frac{z}{2}\right) z^{\mu+\frac{1}{2}}\, {}_1F_1\left(\mu - \kappa + \frac{1}{2}, 1 + 2\mu; z\right), \tag{29}$$

allowing us to rewrite P_{nl} in terms of the Whittaker M function:

$$\begin{aligned} P_{nl}(\xi) &= \sqrt{\frac{\Gamma(n+l+1)}{n^{2l+1}\Gamma(n-l)}} \frac{\sqrt{n^{2l-1}} M_{n,l+\frac{1}{2}}\left(\frac{2\xi}{n}\right)}{\Gamma(2l+2)} \\ &\equiv g_{nl}\, \frac{\sqrt{n^{2l-1}} M_{n,l+\frac{1}{2}}\left(\frac{2\xi}{n}\right)}{\Gamma(2l+2)}. \end{aligned} \tag{30}$$

We note that the dependence of the Einstein coefficient $B(nl \to n_u l_u)$ for bound-bound transitions on the n_u quantum number of the upper state appears only through the Whittaker M function, hence providing a natural analytical continuation over non-integer values of n_u that we have previously introduced as $\bar{B}(nl \to n_u l_u)$.

For $\varepsilon > 0$, the solutions of the radial Schrödinger Eq. (22) are listed in Seaton (1958). A unique combination of these functions with the appropriate boundary conditions for the present problem, namely that the wavefunction reduces to zero in the origin and its asymptotic form at large r behaves as the wavefunction of a free electron, is presented here:

$$\begin{aligned} \chi_{\varepsilon l}(\xi) &= \frac{1}{\kappa^{l+1}} \sqrt{\frac{\Gamma(l+1+i\kappa)\Gamma(l+1-i\kappa)}{\Gamma(i\kappa)\Gamma(-i\kappa)(1-\exp(2\pi\kappa))}} \frac{(i\kappa)^{l+1} M_{i\kappa,l+\frac{1}{2}}\left(-\frac{2i\xi}{\kappa}\right)}{\sqrt{2}\Gamma(2l+2)} \\ &\equiv h_{\kappa l}\, \frac{(i\kappa)^{l+1} M_{i\kappa,l+\frac{1}{2}}\left(-\frac{2i\xi}{\kappa}\right)}{\sqrt{2}\Gamma(2l+2)}, \end{aligned} \tag{31}$$

where $\kappa \equiv 1/\sqrt{\varepsilon}$.

5. Total absorption coefficient at the Balmer limit

5.1. Continuity of the total absorption coefficient

Using the properties of the Euler gamma function, it is straightforward to check that

$$\lim_{n_u\to\infty} g_{n_u l_u} = \lim_{\kappa\to\infty} h_{\kappa l_f} = 1 \quad \forall l_u = l_f \in \mathbb{Z}_{\geq 0}. \tag{32}$$

In Sect. 4.2 we have noted that the Einstein coefficient $B(nl \to n_u l_u)$ is also well defined for non-integer values of n_u, and in particular, that it is a continuous function of n_u. Hence

$$\lim_{\varepsilon\to 0^-} \mathcal{N}_\mathrm{b}(\varepsilon)\bar{B}(nl \to n_u(\varepsilon) l_u) = \lim_{n_u\to\infty} \mathcal{N}_\mathrm{b}(\varepsilon(n_u))B(nl \to n_u l_u). \tag{33}$$

Now recalling the relation (B.1), namely

$$\lim_{\kappa\to\infty} \kappa^{\mu+\frac{1}{2}} M_{\kappa,\mu}\left(\frac{z}{\kappa}\right) = \lim_{\kappa\to\infty} (i\kappa)^{\mu+\frac{1}{2}} M_{i\kappa,\mu}\left(-\frac{iz}{\kappa}\right), \tag{34}$$

which is demonstrated in Appendix B, and using Eq. (30) for the wavefunction of the bound electron P_{nl} and Eq. (31) for the wavefunction of the free electron $\chi_{\varepsilon\ell}$, we find that

$$\lim_{\varepsilon\to 0^-} \mathcal{N}_\mathrm{b}(\varepsilon)\bar{B}(nl \to n_u l_u) = \lim_{\varepsilon\to 0^+} \mathcal{N}_\mathrm{f}(\varepsilon)B(nl \to \varepsilon l_f), \tag{35}$$

provided that the density of quantum states are taken to be the ones obtained in Eqs. (15) and (16). The equality of Eq. (35) further implies the interchange of the limits with the radial integrals contained in the Einstein B coefficients, whose justification is similar to the proof of Eq. (B.1). For brevity, we do not repeat all the computations here. Some additional details are provided in the final note of Appendix B, however.

After summing the bound-bound contributions to Eq. (11) over l and l_u and the bound-free contributions to Eq. (12) over l and l_f, we obtain our final result,

$$\lim_{\nu\to\nu_{\rm th}^-}[\eta(\nu)]_{\rm bb} = \lim_{\nu\to\nu_{\rm th}^+}[\eta(\nu)]_{\rm bf}\,, \tag{36}$$

with the threshold frequency for the Balmer series given by

$$\nu_{\rm th} = \frac{m_e e_0^4}{16\pi\hbar^3}. \tag{37}$$

Thus, we have proven that there is no discontinuity at the Balmer limit.

5.2. Analytic expression for the total absorption coefficient

The wavefunction of the free electron with zero kinetic energy can be calculated combining Eqs. (31) and (B.1):

$$\chi_{\varepsilon=0,\ell}(r) = \frac{(2r)^{\ell+1}\,{}_0F_1(2\ell+2;-2r)}{\sqrt{2}\Gamma(2\ell+2)}. \tag{38}$$

The integrals of Eqs. (19) and (21) can be computed analytically. If we take the limiting wavefunction for the free electron, Eq. (38), and we consider the bound electron to be in the level $n = 2$, we find the nondimensional expressions of Eq. (25):

$$\begin{aligned}
\mathcal{J}(n=2, L_\ell=0; \varepsilon=0, \ell=1) &= \frac{2^8}{e^4},\\
\mathcal{J}(n=2, L_\ell=1; \varepsilon=0, \ell=0) &= \frac{2^7}{\sqrt{3}e^4},\\
\mathcal{J}(n=2, L_\ell=1; \varepsilon=0, \ell=2) &= \frac{2^9}{\sqrt{3}e^4}.
\end{aligned} \tag{39}$$

These are the only non-vanishing integrals, according to the selection rule $\Delta\ell = \pm 1$. Now inserting the reduced matrix (20) into Eq. (17), we compute the Einstein coefficients (where we have substituted the corresponding nondimensional radial integrals $\mathcal{J}$):

$$B(nL_\ell \to \varepsilon\ell) = \frac{2h^2}{3ce_0^2m_e^2}(2\ell+1)\begin{pmatrix} L_\ell & \ell & 1\\ 0 & 0 & 0\end{pmatrix}^2 \mathcal{J}^2(nL_\ell, \varepsilon\ell). \tag{40}$$

For $n = 2$ we can sum over all values of all contributions from the angular momentum of the bound and free electrons, in order to obtain the absorption coefficient at the Balmer limit. Next, we note that the 3-j symbol for $\ell = L_\ell \pm 1$ can be computed using the property

$$\begin{pmatrix} a & a+1 & 1\\ \alpha & -\alpha & 0\end{pmatrix} = (-1)^{a-\alpha-1}\sqrt{\frac{(a-\alpha+1)(a+\alpha+1)}{(a+1)(2a+1)(2a+3)}}, \tag{41}$$

and the fact that squares of 3-j symbols are invariant under permutation of any two columns:

$$(2\ell+1)\begin{pmatrix} L_\ell & \ell & 1\\ 0 & 0 & 0\end{pmatrix}^2 = \frac{\max(L_\ell,\ell)}{2L_\ell+1}. \tag{42}$$

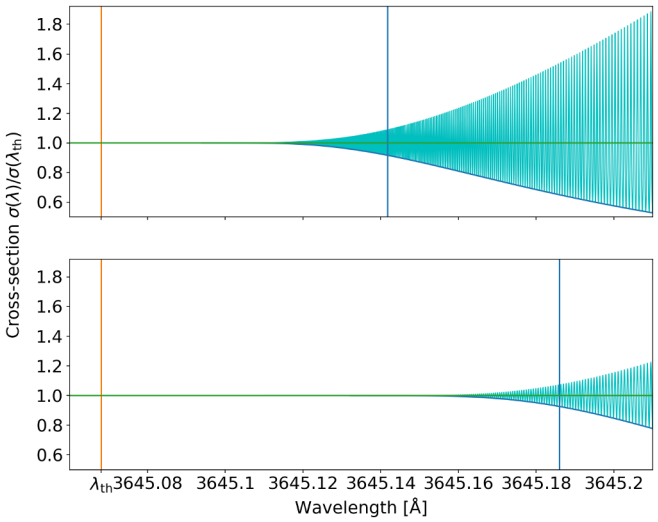

Fig. 1. Total cross-section (cyan) due to bound-bound and bound-free transitions in the isolated hydrogen atom around the Balmer limit $\lambda_{\rm th}$, considering natural broadening (*top*), or including both natural broadening and Gaussian broadening for a thermal velocity of 15 m s^{-1} (*bottom*). The cross-section is normalized to its analytic value at the Balmer limit $\lambda_{\rm th}$. At longer wavelengths, the actual continuum (blue curve), defined as the lower envelope of the bound-bound cross-section, deviates from the nominal quasi-continuum (almost-horizontal green curve that was computed by assuming the approximation of Eq. (10) to be valid at all wavelengths $\lambda > \lambda_{\rm th}$). The orange vertical solid lines show the location of the Balmer limit $\lambda_{\rm th}$. The blue vertical lines show the location at which the FWHM of spectral lines and the separation between consecutive spectral lines are equal (λ_t). In the bottom plot, this line is displaced to longer wavelength due to the additional broadening caused by the thermal velocity.

Making use of Eqs. (8) and (9), summing over the final states, and converting the density of quantum states into c.g.s units finally leads us to

$$\eta_0^{\rm A}(\nu_{\rm th}) = \frac{h^6\nu_{\rm th}}{12\pi^3 ce_0^6m_e^3}\left(\mathcal{N}_{n=2;\,L_\ell=0}\frac{2^{16}}{e^8} + \mathcal{N}_{n=2;\,L_\ell=1}\left(\frac{2^{14}}{9e^8}+\frac{2^{19}}{9e^8}\right)\right). \tag{43}$$

Using the Boltzmann equation, we obtain the relative populations of the $n = 2$ level:

$$\frac{\mathcal{N}_{n=2;\,L_\ell=0}}{\mathcal{N}_{n=2}} = \frac{1}{4}, \quad \frac{\mathcal{N}_{n=2;\,L_\ell=1}}{\mathcal{N}_{n=2}} = \frac{3}{4}, \tag{44}$$

providing the final result:

$$\begin{aligned}
\eta_0^{\rm A}(\nu_{\rm th}) &= \mathcal{N}_{n=2}\frac{h^6\nu_{\rm th}(n=2)}{12\pi^3 ce_0^6m_e^3}\frac{2^{12}\times 3\times 5}{e^8}\\
&= \mathcal{N}_{n=2}\frac{4\pi^2}{3}\left(\frac{\alpha a_0^2}{n^2}\right)_{n=2}\frac{2^{12}\times 3\times 5}{e^8}\\
&\approx \mathcal{N}_{n=2}\times 1.386\times 10^{-17}\,[{\rm cm}^2],
\end{aligned} \tag{45}$$

in which we have introduced the frequency at the Balmer limit given in Eq. (37), and where a_0 is the Bohr radius and $\alpha = e_0^2/(\hbar c) \approx 1/137$ is the fine structure constant.

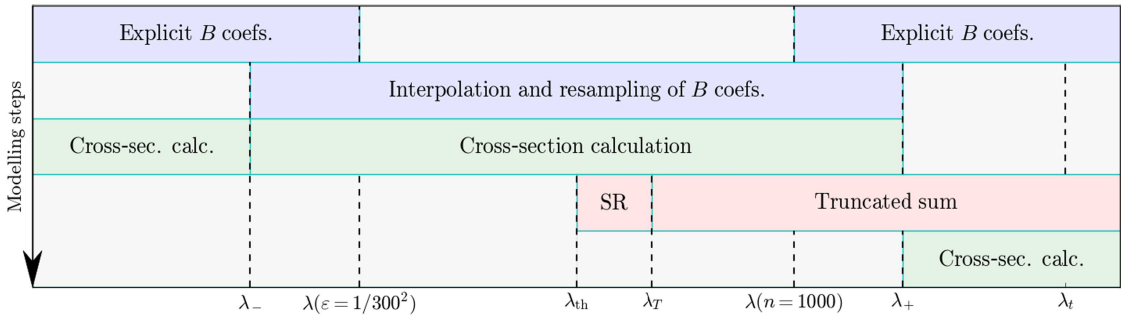

Fig. 2. Steps involved in the modelling of the total cross-section around the Balmer limit. The Einstein B coefficients are first calculated, either explicitly or by interpolation (blue). The cross-section is then computed for $\lambda < \lambda_+$ (upper green region) using either Eq. (11) or Eq. (12). For $\lambda > \lambda_+$, the distance between lines is comparable to the line's FWHM, so that the approximation of Eq. (10) is no longer valid, and lines have to be computed individually, considering both a finite truncated sum and its sum remainder (SR; red). The opacity of the lines is finally summed at wavelengths $\lambda > \lambda_+$ (lower green region).

6. Numerical modelling of the total cross-section around the Balmer limit

At some point near the Balmer limit, the distance between consecutive spectral lines becomes smaller than the width of the lines (FWHM). The exact location of this wavelength λ_t representing the transition between these two regimes depends on the broadening of the spectral lines. At wavelengths longer than λ_t, we still observe distinct spectral lines, but at shorter wavelengths, we no longer resolve spectral lines, but observe a quasi-continuum.

In the following paragraphs we describe the procedure we used to numerically compute the total cross-section in the vicinity of the Balmer limit (Fig. 1). The total Balmer cross-section is defined by

$$\sigma_{\rm Bal.}(\nu) = \frac{h^2\nu}{4\pi} \sum_{\ell} \left(\frac{\mathcal{N}_{n=2;\, l=0}}{\mathcal{N}_{n=2}} \bar{B}(n=2; l=0 \rightarrow \epsilon_0 \ell) + \frac{\mathcal{N}_{n=2;\, l=1}}{\mathcal{N}_{n=2}} \bar{B}(n=2; l=1 \rightarrow \epsilon_0 \ell) \right), \tag{46}$$

where ℓ stands here for either l_u or l_f, and the relative populations of the $n = 2$ level are taken to be the same as in Eq. (44), with l being a shorthand notation for the angular momentum of the lower lever L_ℓ. The procedure to compute this cross-section is non-trivial because the wavefunctions of both the free and bound electrons have singularities at the Balmer limit, leading to numerical difficulties around this region. Moreover, the number of spectral lines to be considered is in principle infinite. The total cross-section at wavelengths larger than the wavelength of the Balmer limit ($\lambda_{\rm th}$) is given as an infinite sum of cross-sections due to each transition from the second level to any higher level. Approaching (from larger wavelengths) the specific point where the line width and the spacing between neighbouring lines are comparable ($\lambda = \lambda_t$), this sum cannot be truncated because the remaining terms are non-negligible and their sum decreases extremely slowly when the truncation threshold increases. However, it is possible to split the sum into two terms, one containing a sum over a finite number of spectral lines located at wavelengths longer than some threshold, λ_T, and one containing an infinite sum over spectral lines located at shorter wavelengths (between $\lambda_{\rm th}$ and λ_T). The infinite sum can then be approximated by an integral, with the same approach as used in Eq. (10).

The choice of λ_T is quite empirical, but $\lambda_T \ll \lambda_t$ is always required and λ_T has therefore to be adjusted according to the line broadening. In the limit $\lambda_T \rightarrow \lambda_{\rm th}$, where the chosen threshold approaches the Balmer limit, the error arising from the approximation in Eq. (10) drops to zero, but the number of lines for which the Einstein coefficient has to be explicitly computed increases drastically. Moreover, close to the limit $\lambda_{\rm th}$, both below and above it, numerical evaluation at finite precision of the Einstein B coefficients is troublesome (see e.g. Morabito et al. 2014). For simplicity, in the present work, we explicitly compute the Einstein B coefficients inside a safe range (for 1000 bound-bound transitions and 300 bound-free transitions) and interpolate its values for transitions closer to the limit. More precisely, we interpolate the values of $\mathcal{N}_{\rm b}(\varepsilon)B(nl \rightarrow n_u l_u)$ together with those of $\mathcal{N}_{\rm f}(\varepsilon)B(nl \rightarrow \varepsilon l_f)$, since we know, according to Eq. (35), that they match at the Balmer limit. The evaluation of the Einstein B coefficients is illustrated in blue in Fig. 2.

The wavelength range in which we perform the numerical calculation of the total cross-section is finally split into three sub-domains, represented in green in Fig. 2: $\lambda < \lambda_-$, for which Eq. (12) is used; $\lambda_- \leq \lambda < \lambda_+$, for which either Eq. (11) or Eq. (12) are used, but the Einstein B coefficients have interpolated and resampled values; and $\lambda \geq \lambda_+$, for which the sum in Eq. (8) is truncated. The truncated part includes a total of 5000 bound-bound transitions, most of which were computed with the interpolated B coefficients, and the remainder of the sum is approximated using Eq. (10), in which all B coefficients are interpolated (SR). This is schematically represented by the red domains in Fig. 2.

We note that for $\lambda < \lambda_{\rm th}$, the total cross-section varies very slowly, so that the choice of λ_- is not really important as the interpolation between λ_- and $\lambda_{\rm th}$ will provide accurate results. However, λ_T should be chosen as close as possible to $\lambda_{\rm th}$ and should satisfy both $\lambda_T \ll \lambda_t$ and $\lambda_T \ll \lambda_+$ to obtain an accurate total cross-section, requiring an explicit computation of a large number of lines. The considered 1000 bound-bound transitions with the Einstein B coefficients computed explicitly is not sufficient, and additional transitions (till $n_u = 5000$, corresponding to λ_T) are considered using the interpolated Einstein B coefficients.

For line transitions to a higher level with quantum number n_u above the $n_u = 81$ threshold, the natural broadening of the lines is extrapolated. Below that threshold, the natural broadening is explicitly computed using Eq. (6.59b) in Landi Degl'Innocenti & Landolfi (2004) (see Fig. 3):

$$\Gamma = \frac{\gamma_{\rm l} + \gamma_{\rm u}}{4\pi}, \tag{47}$$

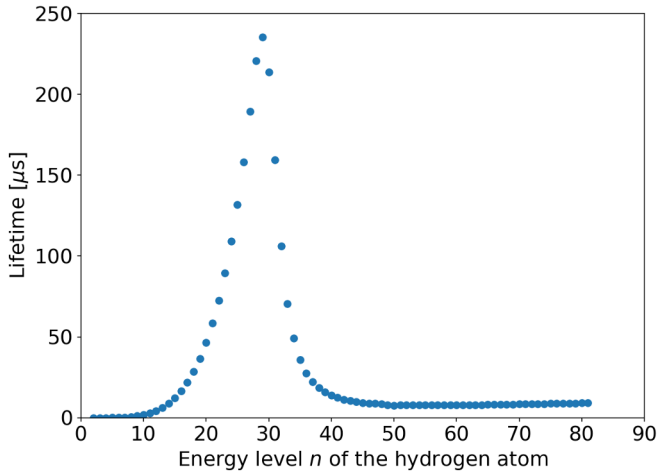

Fig. 3. Lifetimes of the atomic levels n of the hydrogen atom for $1 < n < 82$.

where γ_l and γ_u are the inverse lifetimes of the lower and upper levels. The inverse lifetimes are given by the effective Einstein A coefficients, which are computed using Eq. (63.8) in Bethe & Salpeter (1957) and the usual relations between the Einstein A and B coefficients. Above $n_u = 81$, the extrapolation is carried out by fitting a (semi-empirical) power law $\gamma_u(n) \sim an^{-b}$.

Figure 1 was produced using the methods described above. It is not to be directly compared to a realistic plasma, but it exhibits some characteristic features that are expected to be found in observations as well. First of all, no discontinuity is found anywhere, and in particular, nothing special occurs at the Balmer limit. However, the lower envelope of the spectral lines, interpreted as the "continuum", quickly drops to lower cross-sections. On a spectrum exhibiting a wider range of wavelengths, it would almost appear as a "jump".

The location of the jump is not well defined. Longward of the Balmer limit, close inspection indeed reveals the existence of oscillations up to the limit. With a limited spectral resolution, however, there will be a wavelength shortward of which the oscillating cross-section (lines) become a quasi-continuum. In Fig. 1 the vertical blue line on the right of each panel is the position at which the FWHM of spectral lines is equal to the line separation, and it could be taken as the definition of the Balmer's jump position.

By comparing the plot in the top panel of Fig. 1 (no thermal broadening) with the plot in the bottom panel (thermal broadening corresponding to a thermal velocity of 15 m s^{-1}), we see that the (rather arbitrary) point in which the lines become a quasi-continuum is displaced towards longer wavelengths. The position of this point is very sensitive to the broadening mechanisms that are considered. In the solar plasma, with a temperature of about 6200 K (as expected at the depth at which the solar continuum is formed), and considering only natural and thermal broadening, we expect a displacement of the Balmer jump of approximately 7 Å.

We note that an alternative definition of the Balmer jump is given in Stenflo (2005), according to which the Balmer jump is located at the wavelength on which the Balmer continuum (lower envelope of spectral lines in Fig. 1) intersects the Lyman continuum. This alternative definition has the advantage to better fit what visually looks like the Balmer jump of the intensity spectrum of the Sun, and is located at wavelengths much longer than our definition (in the cited paper, for solar conditions and taking also pressure broadening mechanisms into account, the position is reported to be shifted by 140 Å, while a shift of 100 Å is reported from observational data).

We emphasize that the Gaussian broadening displayed in the bottom panel of Fig. 1 is not representative of any specific plasma. Its only purpose is to provide a qualitative description of the effect of additional broadening. In addition to the thermal Gaussian broadening (Doppler broadening), the interaction between the almost-free electrons close to the photoionization threshold and the electric field of the surrounding ions and electrons in a realistic plasma has to be taken into account (see e.g. Griem 1960). The electric field is not only responsible for the usual linear and quadratic Stark broadening (which rapidly increases with the principal quantum number of the levels), but it also provides an unbounded contribution to the Hamiltonian, which results in the quenching of the lines with high upper quantum number n. This latter aspect has been studied by Lanczos (1931), and it is also described at the end of the chapter on the Stark effect in the book of Bethe & Salpeter (1957).

7. Conclusion

The Balmer jump is produced by a rapid drop of the total Balmer cross-section, but this variation is smooth and continuous when both bound-bound and bound-free processes are taken into account, and its shape and location are dependent on how it is defined and on the broadening mechanisms. A possible definition of the position of the Balmer jump is the location at which the distance between consecutive spectral lines equals the FWHM of the spectral lines. In this work, we have considered an isolated hydrogen atom (no collisions), and we have found that this location is shifted about 7 Å longward of the Balmer limit when considering thermal broadening under solar conditions with respect to the ideal situation in which only natural broadening comes into play.

Moreover, we have shown that at specific wavelengths, and in particular at the Balmer limit, it is possible to compute the cross-section in a fully analytical way. At the Balmer limit, we found this value to be proportional to αa_0^2, with α being the fine-structure constant, a_0 being the Bohr radius, and the proportionality constant being the pure mathematical constant $\pi^2\, 2^{12} \times 5/\exp(8)$.

We proposed a method to deal numerically with the accumulation of an infinite amount of lines and applied it to the simple case of the hydrogen atom near the Balmer limit. We expect this method to be also applicable to the accumulation of spectral lines formed by more complex atoms or molecules. The modelling of the spectrum near the Balmer limit, taking the interactions with the surrounding plasma into account, is expected to be significantly more complex than the present approach and is therefore left for a future work.

Acknowledgements. We are grateful to Edgar S. Carlin for his help with the computation of the reduced matrix elements of the dipole operator, and to Jhih-Huang Li for his revision of the derivations of the asymptotic properties of the Whittaker M function. We are also very grateful to Jiří Štěpán and Roberto Casini for a preliminary reviewing of this work and for providing new ideas and useful feedback, as well as to Javier Trujillo Bueno for inspiring discussions. We also acknowledge the referee's valuable and encouraging input. This work was supported by the Swiss National Science Foundation under grant ID 200020_157103/1.

Note added in proof. We call the reader's attention to the fact that Menzel & Pekeris (1935) and references therein studied the limit $n_u \to \infty$ for the wavefunction of the bound electron and came to the conclusion that there was exact continuity of the absorption

coefficient at the Balmer limit. In the present paper, we used the modern formalism of Landi Degl'Innocenti & Landolfi (2004) to prove continuity.

References

Abramowitz, M., & Stegun, I. 1964, Handbook of Mathematical Functions: With Formulas, Graphs, and Mathematical Tables, Applied mathematics series (New York: Dover Publications)

Bethe, H. A., & Salpeter, E. E. 1957, Quantum Mechanics of One- and Two-Electron Atoms (New York: Academic Press)

Burgess, A., & Seaton, M. J. 1960, MNRAS, 120, 121

Gordon, W. 1929, Ann. Phys., 394, 1031

Griem, H. R. 1960, ApJ, 132, 883

Griffiths, D. J. 1995, Introduction to Quantum Mechanics (Prentice Hall)

Lanczos, C. 1931, Z. Phys., 68, 204

Landi Degl'Innocenti E. 2014, Atomic Spectroscopy and Radiative Processes (Milan: Springer-Verlag)

Landi Degl'Innocenti, E., & Landolfi, M. 2004, Polarization in Spectral Lines, Astrophys. Space Sci. Lib., 307 (Dordrecht: Kluwer Academic Publishers)

Lebedev, N., & Silverman, R. 1965, Special Functions and Their Application, Selected Russian publications in the mathematical sciences (New Jersey: Englewood Cliffs)

Menzel, D. H. 1964, Rev. Mod. Phys., 36, 613

Menzel, D. H., & Pekeris, C. L. 1935, MNRAS, 96, 77

Morabito, L. K., van Harten, G., Salgado, F., et al. 2014, MNRAS, 441, 2855

Seaton, M. J. 1958, MNRAS, 118, 504

Stenflo, J. O. 2005, A&A, 429, 713

Appendix A: Reduced matrix elements of the dipole operator

The reduced matrix elements $\langle \alpha J \,\|\, \boldsymbol{d} \,\|\, \alpha' J' \rangle$ of the dipole operator $\boldsymbol{d} = -e_0 \boldsymbol{r}$ can be expressed in terms of a radial integral in a quite general way by assuming that the quantum numbers contained in α and α' are eigenvalues of operators commuting with angular momentum. We start from the Wigner–Eckart theorem as given in Eq. (2.96) of Landi Degl'Innocenti & Landolfi (2004):

$$\left\langle \alpha J M \left| T^k_q \right| \alpha' J' M' \right\rangle = (-1)^{J'+k+M} \sqrt{2J+1} \begin{pmatrix} J & J' & k \\ -M & M' & q \end{pmatrix} \left\langle \alpha J \left\| \boldsymbol{T}^k \right\| \alpha' J' \right\rangle, \tag{A.1}$$

which is inverted using the orthogonality relations of the 3-j symbols:

$$\left\langle \alpha J \left\| \boldsymbol{T}^k \right\| \alpha' J' \right\rangle = (-1)^{J'+k+M} \sqrt{2J+1} \times \sum_{M' q} \begin{pmatrix} J & J' & k \\ -M & M' & q \end{pmatrix} \left\langle \alpha J M \left| T^k_q \right| \alpha' J' M' \right\rangle, \tag{A.2}$$

and which holds for any $M \in \{-J, -J+1, \ldots, J-1, J\}$. By definition, an irreducible spherical vector rotates with the same transformation law as the $l = 1$ components of the spherical harmonics Y^m_l. Hence, from the components (T_x, T_y, T_z) of an arbitrary Cartesian vector $\boldsymbol{T}$ with norm T, we can construct a spherical vector whose components are given by $cT Y^m_1(\boldsymbol{T}/T)$, with c an arbitrary constant.

Fixing c provides a one-to-one relation between Cartesian vectors and irreducible spherical vectors. For consistency with Eq. (17), the constant is chosen so that the spherical components of the vector field operator $\boldsymbol{r}$ are given by Eq. (2.82) of Landi Degl'Innocenti & Landolfi (2004):

$$r^1_m = \sqrt{\frac{4\pi}{3}} r Y^m_1(\hat{\boldsymbol{r}}), \tag{A.3}$$

which is inserted in the inverted version of the Wigner–Eckart theorem. After setting $M = 0$, the resulting expression reads

$$\langle \alpha J \,\|\, \boldsymbol{d} \,\|\, \alpha' J' \rangle = e_0 (-1)^{J'+1} \sqrt{2J+1}\, \langle \alpha \,|\, r \,|\, \alpha' \rangle \times \sqrt{\frac{4\pi}{3}} \sum_{M' q} \begin{pmatrix} J & J' & 1 \\ 0 & M' & q \end{pmatrix} \left\langle J 0 \left| Y^q_1(\hat{\boldsymbol{r}}) \right| J' M' \right\rangle. \tag{A.4}$$

The angular integrals can be computed using Weyl's theorem (see e.g. relation (8.8) of Landi Degl'Innocenti 2014), resulting in

$$\langle \alpha J \,\|\, \boldsymbol{d} \,\|\, \alpha' J' \rangle = e_0 (-1)^{J'+1} \sqrt{2J'+1} \times \langle \alpha \,|\, r \,|\, \alpha' \rangle \times \begin{pmatrix} J & J' & 1 \\ 0 & 0 & 0 \end{pmatrix} \sum_{M' q} (2J+1) \begin{pmatrix} J & J' & 1 \\ 0 & M' & q \end{pmatrix}^2. \tag{A.5}$$

Using properties of the 3-j symbols, it is possible to check that the sum in the previous relation is equal to 1, leading to our final result

$$\langle \alpha J \,\|\, \boldsymbol{d} \,\|\, \alpha' J' \rangle = e_0 (-1)^{J'+1} \sqrt{2J'+1} \begin{pmatrix} J & J' & 1 \\ 0 & 0 & 0 \end{pmatrix} \times \langle \alpha \,|\, r \,|\, \alpha' \rangle. \tag{A.6}$$

Appendix B: Asymptotic properties of the Whittaker M function

We show that

$$\lim_{\kappa \to \infty} \kappa^{\mu+\frac{1}{2}} M_{\kappa,\mu}\left(\frac{z}{\kappa}\right) = \lim_{\kappa \to \infty} (i\kappa)^{\mu+\frac{1}{2}} M_{i\kappa,\mu}\left(-\frac{iz}{\kappa}\right) = z^{\mu+\frac{1}{2}}\, {}_0F_1(1+2\mu; -z) \tag{B.1}$$

for $\mu \in \mathbb{C}$. The hypergeometric function ${}_0F_1$ is defined by the series

$${}_0F_1(\gamma; z) = \sum_{k=0}^{\infty} \frac{1}{(\gamma)_k} \frac{z^k}{k!}, \quad (\gamma)_k \equiv \gamma(\gamma-1)(\gamma-2)\cdots(\gamma-k+1), \tag{B.2}$$

and the Whittaker M function is defined by

$$M_{\kappa,\mu}(z) = \exp\left(-\frac{z}{2}\right) z^{\mu+\frac{1}{2}}\, {}_1F_1\left(\mu - \kappa + \frac{1}{2}, 1+2\mu; z\right). \tag{B.3}$$

The confluent hypergeometric function ${}_1F_1$ is studied in detail in Lebedev & Silverman (1965) and defined by the hypergeometric series

$${}_1F_1(\alpha, \gamma; z) = \sum_{k=0}^{\infty} \frac{(\alpha)_k}{(\gamma)_k} \frac{z^k}{k!}, \quad \alpha, \gamma, z \in \mathbb{C}, \quad \gamma \neq 0, -1, -2, \ldots \tag{B.4}$$

In particular, ${}_1F_1$ is an entire function of z and of its parameter α, and a meromorphic function of γ with simple poles on points $\gamma = 0, -1, -2$, etc.

We first wish to calculate the asymptotic behaviour of ${}_1F_1\left(a+\kappa, \gamma; \frac{z}{\kappa}\right)$ when $\kappa \to \pm\infty$ for fixed complex numbers a and z and $\gamma \neq 0, -1, -2$, etc. To this aim, we use the dominated convergence theorem applied to the measure space $(\mathbb{Z}_{\geq 0}, \Sigma, \mu)$, with $\Sigma = \mathcal{P}(\mathbb{Z}_{\geq 0})$ the power set of $\mathbb{Z}_{\geq 0}$ and μ the counting measure. With these specific choices, the dominated convergence theorem states that this limit can be computed term by term in the series expansion of ${}_1F_1$, as long as there exists a bounding function $B(k)$ such that for some finite number K

$$\left| \frac{(a+\kappa)_k}{(\gamma)_k} \frac{1}{\kappa^k} \right| \leq B(k) \quad \forall\, |\kappa| > K, \tag{B.5}$$

with $B(k)$ independent of κ, and the series

$$\sum_{k=0}^{\infty} B(k) \frac{|z|^k}{k!} < \infty. \tag{B.6}$$

A bounding function like this can be found for $|\kappa| > |a|$, $|a+\kappa| > |\gamma|$ and $|a+\kappa| > |\gamma|^2$ (we choose for example $K = 1 + |a| + |\gamma| + |\gamma|^2$),

$$\begin{aligned}\left|\frac{(a+\kappa)_k}{(\gamma)_k}\frac{1}{\kappa^k}\right| &= \left|\frac{1\left(1+\frac{1}{a+\kappa}\right)\cdots\left(1+\frac{k-1}{a+\kappa}\right)}{1\left(1+\frac{1}{\gamma}\right)\cdots\left(1+\frac{k-1}{\gamma}\right)}\frac{\left(1+\frac{a}{\kappa}\right)^k}{\gamma^k}\right| \\ &\leq \sup_{n\in\mathbb{Z}_{\geq 0}}\left(\left|\frac{1+\frac{n}{a+\kappa}}{1+\frac{n}{\gamma}}\right|^k\frac{2^k}{|\gamma|^k}\right) \quad (\gamma\neq 0,-1,-2,\dots) \\ &= \sup_{n\in\mathbb{Z}_{\geq 0}}\left(\left|\left(\gamma-\frac{\gamma^2}{a+\kappa}\right)\frac{1}{n+\gamma}+\frac{\gamma}{a+\kappa}\right|^k\frac{2^k}{|\gamma|^k}\right. \\ &\leq \sup_{n\in\mathbb{Z}_{\geq 0}}\left(\left(|\gamma|+\frac{|\gamma|^2}{|a+\kappa|}\right)\frac{1}{|n+\gamma|}+\frac{|\gamma|}{|a+\kappa|}\right)^k\frac{2^k}{|\gamma|^k} \\ &\leq \left(\frac{1+|\gamma|}{d(-\gamma,\mathbb{Z}_{\geq 0})}+1\right)^k\frac{2^k}{|\gamma|^k} \\ &= \left(\frac{2}{|\gamma|}\left(1+\frac{1+|\gamma|}{d(-\gamma,\mathbb{Z}_{\geq 0})}\right)\right)^k \\ &\equiv B(k)\equiv cB^k,\end{aligned} \tag{B.7}$$

where with this bound $c = 1$, and we have defined the distance function for $z \in \mathbb{C}$ and $E \subset \mathbb{C}$ to be given by

$$d(z,E) \equiv \inf_{w\in E}(|z-w|). \tag{B.8}$$

With the bound $B(k)$, it is clear that Eq. (B.6) is satisfied:

$$\sum_{k=0}^{\infty} B(k)\frac{|z|^k}{k!} = c\sum_{k=0}^{\infty} B^k\frac{|z|^k}{k!} = c\cdot\exp(B|z|) < \infty, \tag{B.9}$$

but we note that in the relevant case in which $\gamma \geq 2$ (corresponding to the angular momentum $l \geq 0$), K could be chosen even greater, and with $c = 3/2$, it is possible to find a similar bound for which B is arbitrarily close to $1/3$ (this bound is not required for the present proof, but will be useful later). The limits, term by term in the series expansion of ${}_1F_1$, are finally given by

$$\lim_{\kappa\to\pm\infty}\frac{(a+\kappa)_k}{(\gamma)_k}\frac{1}{\kappa^k} = \frac{1}{(\gamma)_k}, \tag{B.10}$$

and by application of the dominated convergence theorem

$$\lim_{\kappa\to\pm\infty}{}_1F_1\left(a+\kappa,\gamma;\frac{z}{\kappa}\right) = \sum_{k=0}^{\infty}\frac{1}{(\gamma)_k}\frac{z^k}{k!} \equiv {}_0F_1(\gamma;z). \tag{B.11}$$

The same reasoning with the same bound, but substituting $\kappa \to i\kappa$, provides a proof of

$$\lim_{\kappa\to\pm\infty}{}_1F_1\left(a+i\kappa,\gamma;-\frac{iz}{\kappa}\right) = {}_0F_1(\gamma;z). \tag{B.12}$$

The proof of Eq. (B.1) then follows by substituting $\kappa \to -\kappa$ (and $\kappa \to -i\kappa$, respectively), $z \to -z$, $a \to \mu + \frac{1}{2}$ and $\gamma \to 1 + 2\mu$ in Eqs. (B.11) and (B.12), and inserting the resulting limits in Eq. (B.3).

We note that choosing $1/3 < B < 1/2$ further allows us to prove that the wavefunctions of the bound/free electrons are bounded independently of n_u and ε and that the wavefunction of the bound electron is (asymptotically) exponentially decreasing. It is indeed straight-forward to check with this bound that ${}_1F_1$ in Eq. (B.3) grows more slowly than $\exp(z/2)$, allowing an exponential decay of the Whittaker M function in Eq. (B.3). Hence the integrands inside the radial integrals (19) and (21) are also bounded and (asymptotically) exponentially decreasing. Using again the dominated convergence theorem, we can further justify the interchange of the limits $n_u \to \infty$ (and $\varepsilon \to 0$ respectively) and the radial integrals.